Structural geometry, electronic structure, thermo-electronic and optical properties of GaCuO2 and GaCu0.94 Fe0.06O2 : a first principle approach of three DFT functionals

8 authors, including:

Debashis Howlader
European University of Bangladesh, Dhaka, Bangladesh
15 PUBLICATIONS **91** CITATIONS

Md. Sayed Hossain
Bangladesh Atomic Energy Commission
14 PUBLICATIONS **34** CITATIONS

Unesco Chakma
European University of Bangladesh
37 PUBLICATIONS **139** CITATIONS

Ajoy Kumer
European University of Bangladesh
**92** PUBLICATIONS **444** CITATIONS

Some of the authors of this publication are also working on these related projects:

Project A Computational Investigation of Electronic Structure and Optical Properties of AlCuO2 and AlCu0.96Fe0.04O2: A First Principle Approach View project

Project Prediction the thermophysical properties, chemical reactivity, and biological study for Ionic Liquids, natural products, organomatallic crystal and dye. View project
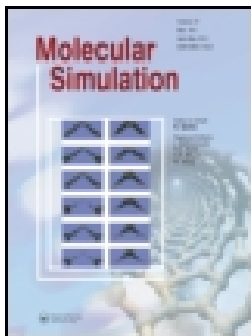
Structural geometry, electronic structure, thermo-electronic and optical properties of GaCuO$_2$ and GaCu$_{0.94}$Fe$_{0.06}$O$_2$: a first principle approach of three DFT functionals

Debashis Howlader, Md. Sayed Hossain, Unesco Chakma, Ajoy Kumer, Mohammad Jahidul Islam, Md. Tawhidul Islam, Tomal Hossain & Jahedul Islam

Published online: 18 Sep 2021.

Submit your article to this journal

View related articles

View Crossmark data

Taylor & Francis
Taylor & Francis Group

Check for updates

Structural geometry, electronic structure, thermo-electronic and optical properties of GaCuO$_2$ and GaCu$_{0.94}$Fe$_{0.06}$O$_2$: a first principle approach of three DFT functionals

Debashis Howlader [a], Md. Sayed Hossain [b], Unesco Chakma [a], Ajoy Kumer [c], Mohammad Jahidul Islam [d], Md. Tawhidul Islam [a], Tomal Hossain [a] and Jahedul Islam [e]

aDepartment of Electrical and Electronics Engineering, European University of Bangladesh, Gabtoli, Dhaka, Bangladesh; bCenter for Research Reactor, Bangladesh Atomic Energy Commission, Dhaka, Bangladesh; cDepartment of Chemistry, European University of Bangladesh, Gabtoli, Dhaka, Bangladesh; dDepartment of Physics, European University of Bangladesh, Dhaka; eDepartment Of Civil Engineering, Presidency University, Dhaka, Bangladesh

ABSTRACT

As Gallium oxides have been using in optoelectronic devices due to its high potentiality and efficiency, therefore, the Gallium–Copper oxide crystal has been computationally designed and screened for its electronic structure, thermo-electronic and optical properties using density functional theory (DFT). To kick off, GGA) with PBE has been implemented for the crucial screening of its structural geometry and the optimisation for both GaCuO$_2$ and GaCu$_{0.94}$Fe$_{0.06}$O$_2$. Afterwards, the electronic structure, thermo-electronic and optical properties were analysed from optimised structures. In addition, for the comparison study of obtained data of the GGA with PBE functional with two DFT functionals, such as LDA with CA-PZ and GGA with RPBE methods have been performed. The band gaps for GaCuO$_2$ are 0.756, 0.786 and 0.759 eV for the GGA with PBE, GGA with RPBE, and LDA with CA-PZ, respectively, whereas it has garnered after 6% Fe doping (GaCu$_{0.94}$Fe$_{0.06}$O$_2$) is at 0.00 eV. And come to think of it, the thermo-electronic and thermophysical properties have been added to endow with the absorption of visible light, thermal stability and thermal state before and after doping which leads to use these crystals in lasers, solar cell even luminescent as optoelectronic materials.

1. Introduction

Semiconductors are a curious class of materials having exclusive electrical characteristics for their potential applications, such as electronic technology [1], power devices [2], nanospintronic devices [3,4], diodes, transistors [5], photo-sensors [6], microcontrollers [7] and integrated circuits [8]. In the contemporary era, most of the electronic technologies and optoelectronic devices solely depend on using of semiconductor materials due to their chemical, physical, thermo-electronic properties [9], good chemical stability [10,11] and optical characters [12–19]. In addition, its low cost and availability have been opening new windows for its applications in medical devices [20], environmental safety equipment [21], chemistry and chemical laboratory testing apparatus [22] and photocatalysts for catalysis chemistry [23–26]. To say more, the organic semiconductor has been developing for modification their chemical structures which are environment friendly and low toxic [27–30], as well as liquids crystal has developed for more flexible uses in electronic technologies [31–33]. However, it is a towering challenge to obtain the high-efficiency semiconductor at room temperature using group II–IV metals because of various applicable moods [34–38]. Among these defects, the atomic size, wide band gap and price are the most attentive point to generate new semiconductor materials, although these have a vast implication to absorb or emit ultraviolet (UV) light in applications of optoelectronic devices [39,40]. Among of all atoms, crystals of Gallium or Gallium oxides have been considered promising candidates for

transparent electronics, chemical and gas sensors, optoelectronic devices [41,42] and UV emitters with wide band gap [43–46].

As there are various structural forms of Gallium oxide crystals, particularly Gallium-based metal alloys have been used in the injection of femtolitre sized samples into cells [47], printed free-standing columns and spheres of EGaIn [48–50], the demand of Cu-based alloys has been placed to researchers to investigate and design new materials with desirable thermo-chemical properties [51–53]. Regarding these prospects with the scope of developing Gallium oxide alloy with jointly Copper metals having a chemical formula, GaCuO$_2$, has been designed for this study to evaluate its electronic structure, structural geometry and optical properties using computational tools. The crucial fact to pick up the Ga and Cu atom deems the smaller atomic size which can give the uncomplicated electronic transition from the valence band to the conduction band; consequently, it creates many free electrons but oxygen produces more free electrons than Ga and Cu atom in GaCuO$_2$ crystal. As a result, the foremost supportive evidence of their outlook uses has to be noted that GaCuO$_2$ is a naturally n-type similar material, and considered as rewarding electrons/current carrier. So that reason, the GaCuO$_2$ might be used as the material in light-emitting diodes (LEDs), lasers, solar cells and nanosensors. On the basis of electron carrier, the main fact is to improve its current conduction while the lowest barrier is expected. Consequently, 6% Fe (GaCu$_{0.94}$Fe$_{0.06}$O$_2$) was doped due to its top-most efficiency to reduce the barrier of electron conduction [19,24,54].

There are no enough theoretical and computational studies about GaCuO$_2$ which makes a scope to examine and screen this crystal through computational tools using DFT. The first principle method has been executed to study GaCuO$_2$ crystal including their structural geometry, electronic structure, optical properties and thermo-electronic properties. Then, the doping is an important method for modulating to apply impurities to make the intrinsic material with its structural, electrical and optical properties. Keeping these issues in mind, the effect of Fe doping on several properties of GaCuO$_2$ has been studied thoroughly for the first time on this crystal. Finally, GGA with PBE, GGA with RPBE and LDA with CA-PZ functionals have been used to make a comparative study to obtain a more accurate magnitude and their acceptance.

2. Computational methods

The GGA with PBE has been adapted from the CASTEP code of Material Studio version 8.0 [55] and is used to calculate band structure, the total density of state (DOS) and partial density of state (PDOS), because it is considered the most reliable and acceptable method for calculating electronic structure and structural features [56]. In this case, the density of state and band structure have been calculated using the cut-off at 510 eV and k point at 2×2×1 with norm-conserving pseudopotentials. Then similarly, the optical properties have been simulated to calculate the reflectivity, absorption, refractive index, dielectric function, conductivity and loss function. Furthermore, the geometric optimisation is achieved before the energy calculation, and the convergence criterion for the force between atoms is at $3×10^{-6}$ eV/Å. The maximum displacement is at $1×10^{-3}$Å, and the total energy and the maximal stress are at $1×10^{-5}$ eV/atom and $5 × 10^{-2}$ GPa, respectively.

The Fe atom has been doped in replacing Cu atoms into the GaCuO$_2$ by 0.06 portions or 6 percentages to obtain the new Fe atom doped metalloid into the parent crystal structure. The crystal structure is in a symmetry pattern that is why the minimum portion of doping by 6% is optimised. Secondly, for comparative research of band gap for GaCuO$_2$ and GaCu$_{0.94}$Fe$_{0.06}$O$_2$, the other two common methods, such as Generalised Gradient Approximation (GGA) with Revised Perdew–Burke–Ernzerhof functional (RPBE), Local Density Approximation (LDA) with Ceperley and Alder, and Perdew and Zunger with (CA-PZ) functionals also have been investigated using required cut-off energy at the same condition.

3. Results and discussion

3.1. Optimised structure

The lattice parameters are a = 3.013 Å, b = 3.013 Å, c = 11.548 Å and angels between them are α = 90.000 Å, β = 90.000 Å, γ = 120.000 Å. The monoclinic GaCuO$_2$ crystal and the area cluster which is Hermanna Mauguin P63/mmc [194], hexagonal crystals system, point cluster 6/mmm, hall -P 6c 2c, density 6.04 g/cm^3 are shown in Figure 1(a) and also the Fe-doped optimised structure is reported in Figure 1(b).

3.2. Electronic structure

The Fermi energy level has been set at zero point for determining the electronic band structures of GaCuO$_2$ and GaCu$_{0.94}$Fe$_{0.06}$O$_2$ by GGA with PBE, GGA with RPBE and LDA with CA-PZ. It is found from Figure 2(a) that the minimum of conduction bands (MCB) is obtained middle points between M and L symmetry points whereas the maximum of valance bands (MVB) is located in the G symmetry point. The symmetry point is seen at different MCB and MVB points, therefore, and the obtained band gap is termed as the indirect band gap, as well as the calculated values are in 0.756 and 0.00 eV for GaCuO$_2$ and GaCu$_{0.96}$Fe$_{0.04}$O$_2$, respectively, using GGA with PBE method. Due to the strong contribution of the d-orbital of the Fe atom within the photon energy range from 0 to 1 eV, the band gap is turned at 0.00 eV. Therefore, after Fe doping into the sample material, it acquires more electron density predicted from DOS and PDOS which leads to a good conducting property, as well as other optical properties are also enhanced. From the demonstration of Figure 2(a), it can be summarised that lower parts of the conduction band are well dispersive which varies from symmetry points P to F whereas it follows the almost steady pattern between the symmetry points G and P. On the other hand, the upper levels of the valance band near the G symmetry point are dispersive, but the lower parts are not such dispersive as the upper parts of GaCuO$_2$. Usually, a lower carrier of effective mass shows higher carrier mobility which leads to estimate the potential materials for high-mobility electronic devices [57].

When the Fe metal is doped into GaCuO$_2$ by 6%, a different band structure has been found which is completely different from GaCuO$_2$. To kick off, the MCB is obtained in the G symmetry point, whereas the MVB is also linked in the G symmetry point. At the G symmetry point from Figure 2(b), the direct band gap is found at 0.00 eV using GGA with PBE.

Due to the addition of Fe atom as a doping element, there is a large change in the upper levels of the conduction bands which are well dispersed at the G symmetry point and the upper band is also decreased as a whole except at Y and D points while in the case of valance band, there are a lot of changes occurred as a whole compared to undoped.

Secondly, another method called GGA with RPBE has been demonstrated to calculate the band gaps by maintaining the same conditions and the corresponding pictorial views are listed in Figure 2(c,d). Figure 2(c,d) indicates that the band gaps are indirect and direct, and the magnitudes are at 0.786 and 0.00 eV for GaCuO$_2$ and GaCu$_{0.94}$Fe$_{0.06}$O$_2$, respectively. Finally, the method of LDA with CA-PZ has been applied for the investigation of band gaps for GaCuO$_2$ and GaCu$_{0.96}$Fe$_{0.04}$O$_2$, and the outputs are presented in Figure 2(e,f), which can be articulated that the indirect and direct band gaps are in 0.759 and 0.00 eV for GaCuO$_2$ and GaCu$_{0.94}$Fe$_{0.06}$O$_2$, respectively. Analysing all the above figures, it can be concluded that all band gaps are deemed as indirect and direct band gaps for GaCuO$_2$ and GaCu$_{0.96}$Fe$_{0.04}$O$_2$, respectively, and the values are almost closer for three methods. The comparative values using the optimised condition are listed in Table 1.
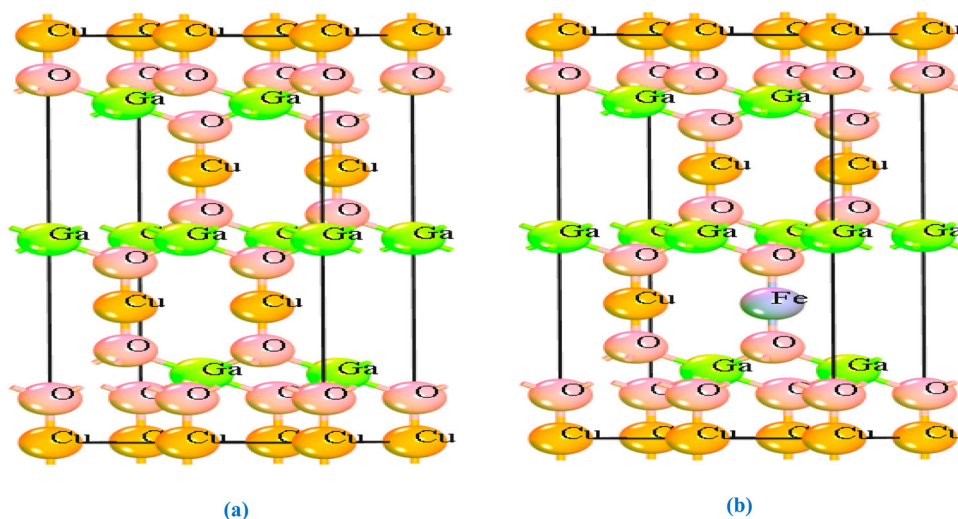
Figure 1. (Colour online). (a) Structure for GaCuO$_2$, (b) structure for GaCu$_{0.96}$Fe$_{0.04}$O$_2$.

3.3. Density of states and partial density of state

The knowledge of the nature of electronic band structures and the scattering of orbitals are obtained by studying the DOS and PDOS. The method of GGA with PBE has been applied to find out the DOS and PDOS of Ga, Cu, Fe and O elements for GaCuO$_2$ and GaCu$_{0.94}$Fe$_{0.06}$O$_2$ crystals.

The comparative study of DOS between GaCuO$_2$ and GaCu$_{0.94}$Fe$_{0.06}$O$_2$ crystals is shown in Figure 3(a) which illustrates that GaCu$_{0.94}$Fe$_{0.06}$O$_2$ confirms the highest electron density in valance band than GaCuO$_2$. The illustration of the PDOS for GaCuO$_2$ is shown in Figure 3(b), and the nature of 4s^2 and 4p^1 for Ga; 3p^6, 3d^{10} and 4s^1 for Cu; 2s^2 and 2p^4 for O elements have been studied to explain the transition of electrons due to hybridisation by travelling from the maximum valence band (MCB) to the minimum conduction band (MCB) from the simulation of DOS. The higher domination among other orbitals comes from the p-orbital in the conduction band, and the d-orbital has the higher contribution for creating the valance band. In the case of Ga, the 4p^1 orbital is almost vacant; therefore, it tends to move towards the conduction band while p-orbital is also partially filled up with 2p^4 for O-atom and 3d^{10} and 4s^1 orbitals for Cu-atom. As a result, the highest peak for PDOS of the conduction band is obtained from the combined contribution of p-orbital at about 2.5 eV and s-orbital at 5 eV. Moreover, the PDOS of p-orbital in conduction band follows the same pattern for DOS. So, it can be said that the conduction band consists of 4p^1 of Ga; 3d^{10} and 4s^1 of Cu; and 2p^4 of O-atom whereas the valence band is made up of a mixer of p-orbital and d-orbital. The maximum intensity or density of electrons of the valence band is about 8.0 electrons/eV while d-orbital is responsible for almost 7.0 electrons/eV. The density of electrons in the conduction band is higher for the s-orbital and p-orbital.

Figure 3(c) demonstrates the PDOS of GaCu$_{0.94}$Fe$_{0.06}$O$_2$, and it consists of 4s^2 and 4p^1 for Ga; 3p^6, 3d^{10} and 4s^1 for Cu; 3d^6 and 4s^2 for Fe and 2s^2 and 2p^4 for O elements. The d-orbital of the Fe atom provides a strong contribution to the conduction band from 0 to 1 eV, whereas the p and s orbitals also provide some contribution to the conduction band at

energies 2.5 and 4 eV, respectively. On the other hand, d and p orbitals have the higher portion for the valance band at energies about 2.5 and 4 eV, respectively. The d-orbital in the conduction band has the most contribution for GaCu$_{0.94}$Fe$_{0.06}$O$_2$ and the doping of Fe reduces the band gap at 0.0 eV. The comparative study of s, p and d orbitals for GaCuO$_2$ and GaCu$_{0.94-}$Fe$_{0.06}$O$_2$ has been depicted in Figure 3(d–h). The contribution of both s and p orbitals in GaCuO$_2$ and GaCu$_{0.94}$Fe$_{0.06}$O$_2$ is almost the same, but it is different for the d-orbital. From the study, it can be said that the d-orbital is the higher contributor of conduction band within the region of 0.0 to 1.0 eV for only GaCu$_{0.94}$Fe$_{0.06}$O$_2$, whereas both p and s orbitals have the contribution for GaCuO$_2$ and GaCu$_{0.94}$Fe$_{0.06}$O$_2$ after 1.0 eV.

3.4. Optical properties

For studying energy band structure, excitations, impurity levels, localised defects and lattice vibrations, the optical properties of solids offer an important tool. The absorption, refractive index, dielectric function $\varepsilon(\omega)$, optical conductivity and loss function have been analysed in order to investigate the optical properties of undoped and Fe-doped GaCuO$_2$ crystals. In such investigations, reflectivity, absorption, refractive index, dielectric function $\varepsilon(\omega)$, optical conductivity and loss function have been illustrated. It is the frequency-dependent complex dielectric function $\varepsilon(\omega)$ or the complex conductivity, which is directly related to the energy band structure of solids. After doping, the photocatalytic behaviours of GaCu$_{0.94}$Fe$_{0.06-}$O$_2$ have been analysed as below.

3.4.1. Optical reflectivity

The formation of periodically spaced vacancy layers within the meta-stable phase of Ga-Cu-O$_2$-based phase-change materials has recently gained a lot of attention since associated electron delocalisation effects induce an insulator–metal transition. For studying primarily, the potential of the vacancy ordering phenomena, it is extremely important to produce the highly ordered meta-stable phase separately from the closely related thermodynamically stable phase.
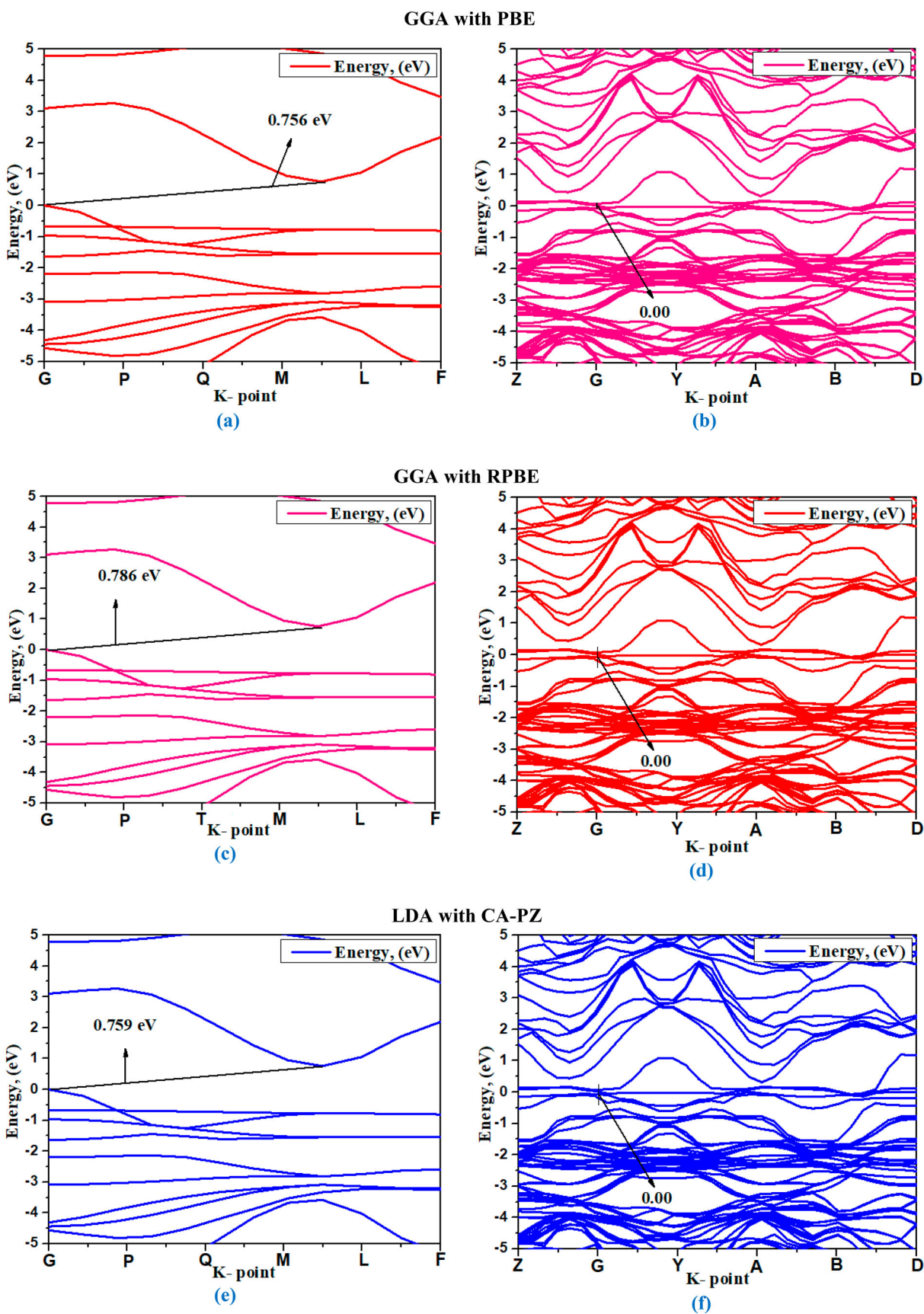
Figure 2. (Colour online). Electronic structure for (a) $GaCuO_2$, (b) $GaCu_{0.96}Fe_{0.04}O_2$, (c) $GaCuO_2$, (d) $GaCu_{0.96}Fe_{0.04}O_2$, (e) $GaCuO_2$ and (f) $GaCu_{0.96}Fe_{0.04}O_2$.

Table 1. Comparative band gaps for GaCuO$_2$ and GaCu$_{0.94}$Fe$_{0.06}$O$_2$.

Compounds name	Analysis methods		
	GGA with PBE	GGA with RPBE	LDA with CA-PZ
GaCuO$_2$	0.756 eV	0.786 eV	0.759 eV
GaCu$_{0.94}$Fe$_{0.06}$O$_2$	0.00 eV	0.00 eV	0.00 eV

To explain the role of electronic transition from the valance band to the conduction band and the absorbance of that material, reflectivity is a key tool that is analysed for incident rays on the surface of the semiconductor. It has been reported in several previous studies that the lower reflectivity conveys the higher UV or visible light absorption [58–60]. In Figure 4, it is seen that the reflectivity of GaCuO$_2$ and GaCu$_{0.94}$Fe$_{0.06}$O$_2$ starts at around 0.15 and 0.18, respectively, from the initial frequency. Afterwards, the reflectivity of GaCuO$_2$ shows lower value before 2.0 eV and the opposite phenomenon is observed after the 2.0 eV. In addition, for GaCuO$_2$, reflectivity increases to about 0.24 and then starts to fall for the corresponding frequency at about 4 eV as illustrated in Figure 4. In the case of GaCu$_{0.94}$Fe$_{0.06}$O$_2$, the reflectivity also changes at the same point but a little bit higher than GaCuO$_2$. From Figures 4 and 5, it is observed that the value of reflectivity is highly lower compared to the absorption.

3.4.2. Absorption

To calculate the optical absorbance of GaCuO$_2$ and GaCu$_{0.94}$Fe$_{0.06}$O$_2$ materials, the polycrystalline polarisation method has been utilised, and a tiny smearing value of 0.1 has been applied to achieve more distinct absorbance peaks.

From Figure 5, it is seen that the absorbance peaks are produced at different photon energies where electronic transitions from MVB to MCB are occurred due to the incident light (visible). Regarding that case, it expresses that the crystal GaCuO$_2$ can be absorbed photons energy of visible range and above the visible range whereas Fe-doped crystal (GaCu$_{0.94}$Fe$_{0.06}$O$_2$) shows on more peaks than undoped, indicating higher absorption. Since absorption is directly related to electromagnetic radiation, it is subject to photon energy. However, Figure 5 demonstrates the comparative study of the absorption for GaCuO$_2$ and GaCu$_{0.94}$Fe$_{0.06}$O$_2$. From the
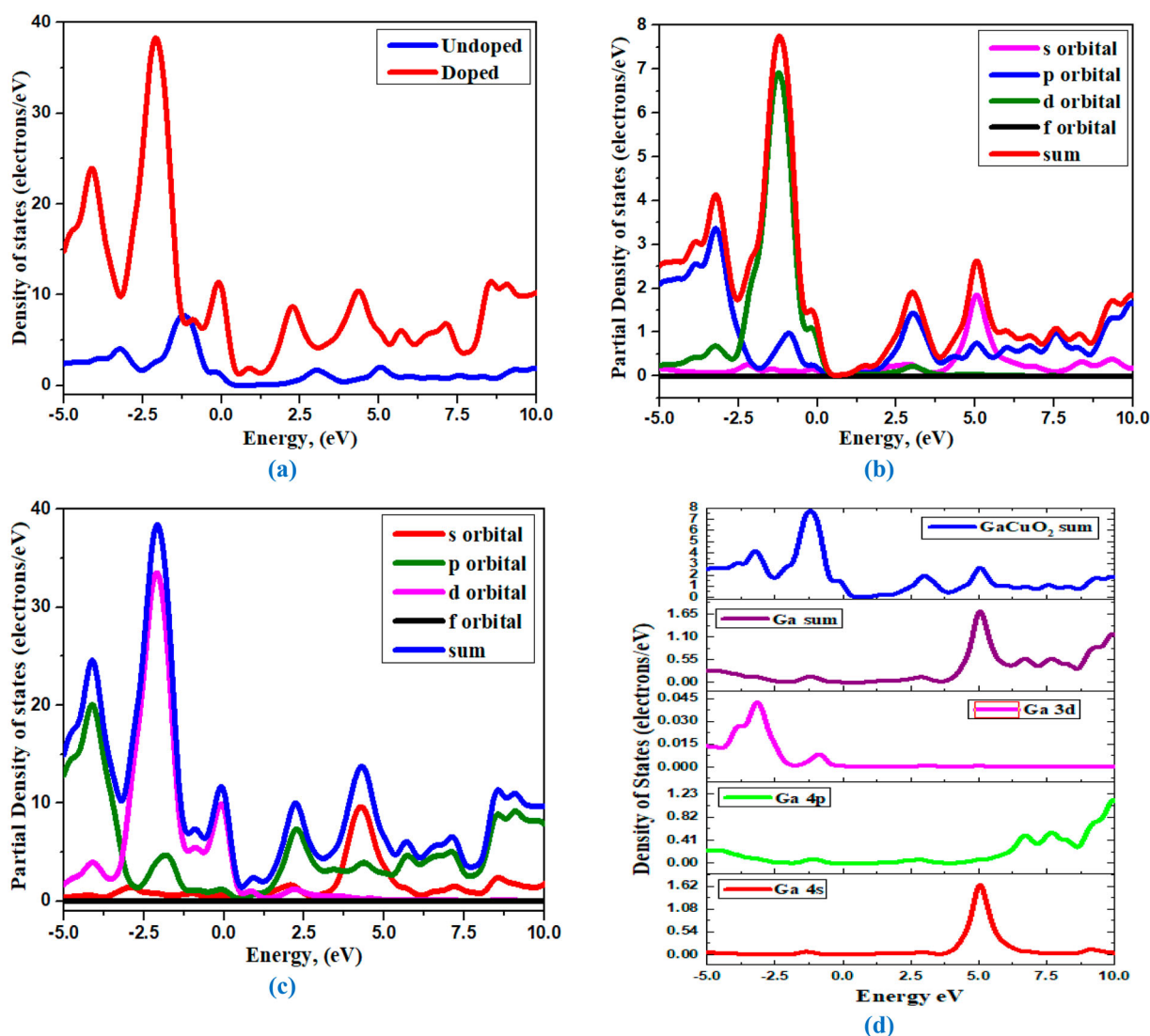

Figure 3. (Colour online). (a) Comparison of total DOS for doped and undoped, (b) PDOS for undoped, (c) PDOS for doped, (d) PDOS of GaCuO$_2$ for Ga atom, (e) PDOS of GaCuO$_2$ for Cu atom, (f) PDOS of GaCu$_{0.94}$Fe$_{0.06}$O$_2$ for Ga atom, (g) PDOS of GaCu$_{0.94}$Fe$_{0.06}$O$_2$ for Cu atom and (h) PDOS of GaCu$_{0.94}$Fe$_{0.06}$O$_2$ for Fe atom.
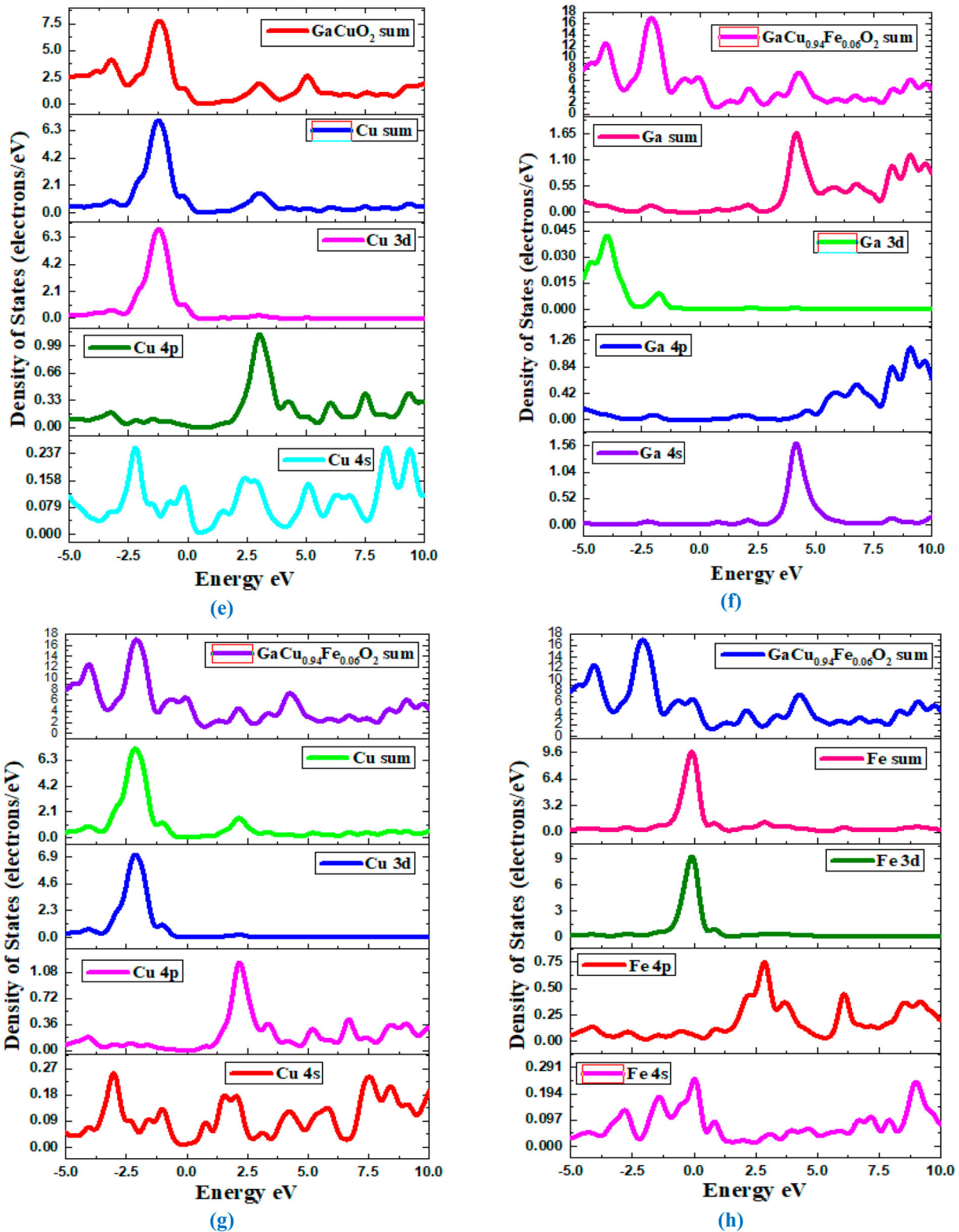
Figure 3 Continued

photon energy level 0.9 to 3 eV, the absorption increases slowly and afterwards, the absorption increases sharply for both cases. Although both the curves of GaCuO$_2$ and GaCu$_{0.94}$Fe$_{0.06}$O$_2$ follow almost the same trend, the absorption level of the doped material is higher from about 1.0 to 3.0 eV and it increases gradually after 4.0 eV. As the doped material gains lower band gap and higher absorption, as well as a wide range of photon energy absorption capabilities just after the initial point, therefore, this material might be used as the materials in the making of the various optical communication devices [61,62]. Thus, after doping, it might make as an additional transom, skylight and windowplane

Figure 4. (Colour online) Reflectivity.

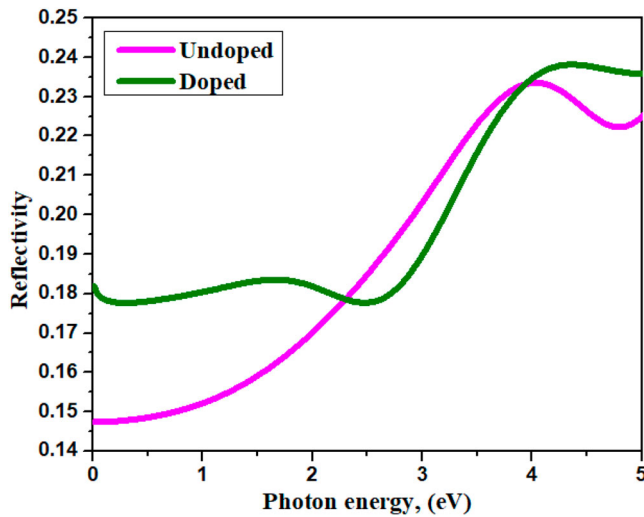**Figure 6.** (Colour online) Refractive index.

for semiconductor materials for uses of optoelectronic devices.

3.4.3. Refractive index

Refractive index, expressing the speed of light in a vacuum to other medium, indicates that a greater refractive index figures out a greater denser medium or lower absorption. Figure 6 displays the refractive index as a function of photon energy. It consists of the real part and the imaginary part and can be defined as the ratio of light speed in free space to the other medium. The larger value of the real part is desirable for application in optoelectronic devices and the phenomenon is inversed for the imaginary part.

At the initial point of photon energy, the refractive index is higher for real parts, while the imaginary part is almost close to zero for both $GaCuO_2$ and $GaCu_{0.94}Fe_{0.06}O_2$. The real parts of the refractive index follow approximately stable trend with increasing photon energies up to 3.5 eV, afterwards they decrease slowly with increasing photon energies. Here, it is
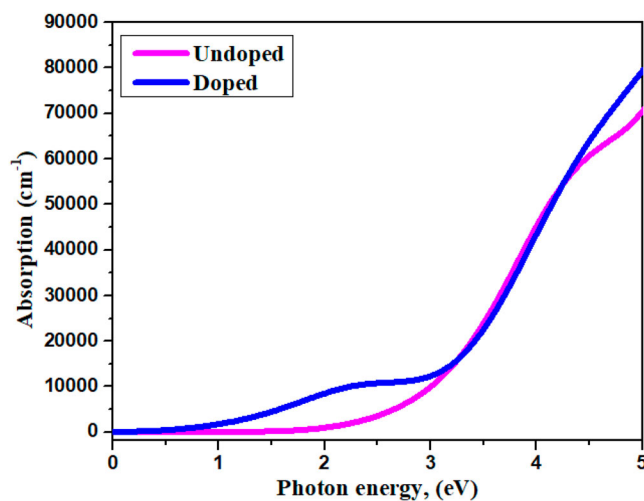

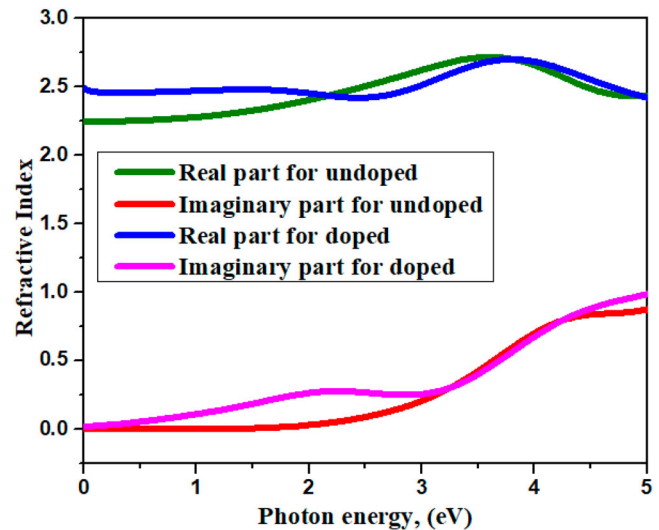**Figure 5.** (Colour online) Absorption.

observed that the real part of $GaCu_{0.94}Fe_{0.06}O_2$ is higher than $GaCuO_2$ up to 2.0 eV, indicating the better usable materials in the expected area, although the band gap has been found at about 0.8 eV.

3.4.4. Dielectric function

The dielectric function is the most indispensable tool for exploring their optical properties which are correlated with adsorption properties for solid as shown in the following equation:

$$(\omega) = \varepsilon_1(\omega) + i\varepsilon_2(\omega)$$

Here, $\varepsilon_1(\omega)$ and $\varepsilon_2(\omega)$ are represented the dielectric constant (real part) and the dielectric loss factor (imaginary part), respectively. The dielectric function is related to the space of materials that is physically compatible with the absolute permittivity or permittivity. The energy storage capability in the electric field is represented by the real part of the dielectric function, whereas the energy dissipation capability of the dielectric materials is represented by the imaginary part. From Figure 7, it is clear that, for both crystals, the real parts of the dielectric function illustrate the larger magnitude, meaning that it can be highly used as an electrostatic cell as energy storage materials. Moreover, $GaCu_{0.94}Fe_{0.06}O_2$ can be a more effective material than $GaCuO_2$ as electrostatic cell material.

3.4.5. Conductivity

Conduction through semiconductors based on energy bands and orbital electrons is related to the distinct space of electrons in orbit. Conduction in semiconductors happens due to the presence of holes and free electrons in the crystal molecules. Figure 8 demonstrates that the conductivity of doped material $GaCu_{0.94}Fe_{0.06}O_2$ is slightly higher than that of the undoped $GaCuO_2$. The real parts increase slowly up to 3.0 eV and after then they increase sharply whereas the imaginary parts decrease following opposite direction with little variation at the end portion. It is also observed that the upper peak of the conductivity reaches about 3.0 1/fs at 5.0 eV for
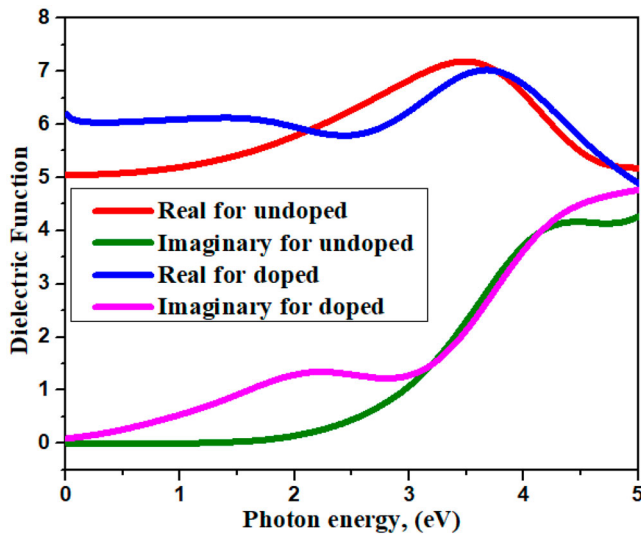
Figure 7. (Colour online) Dielectric function.

Figure 9. (Colour online) Loss function.

$GaCu_{0.94}Fe_{0.06}O_2$. Finally, Figure 8 presents that the conductivity increases after 6% Fe doping.

3.4.6. Loss function

The high energy regions and low energy regions are obtained from the curve of energy. The first region accounts for the high loss energy with frequency or spectral change after ionising edge which can be called oxidation state of *d*-orbital splitting for atomic metals in complex compounds, having a range above 3.5 eV. The other is a low energy loss function below 3.0 eV which can provide information about the composition and electronic structure. From Figure 9, it is represented the loss function for $GaCuO_2$ and $GaCu_{0.94}Fe_{0.06}O_2$. To kick off, the loss function of $GaCu_{0.94}Fe_{0.06}O_2$ is higher than $GaCuO_2$ in the low energy region of which the doping indicates the higher loss of energy for the case of electronic structure and their composition. On the other edge of the loss function, there is a little change for both $GaCuO_2$ and $GaCu_{0.94}Fe_{0.06}O_2$
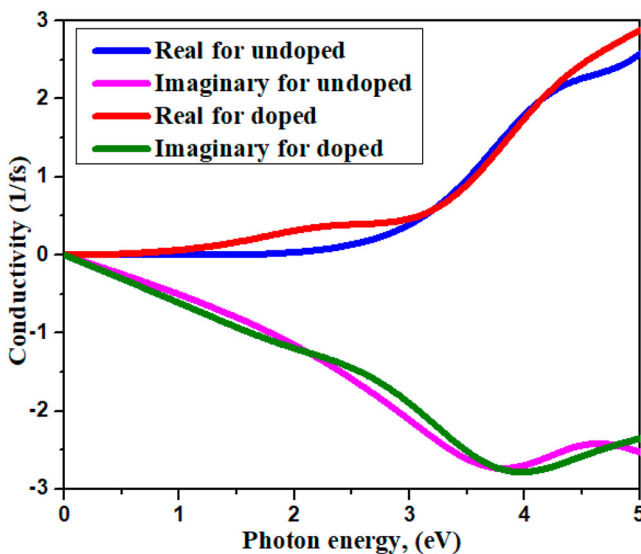
in higher energy part which mentions that there has no difference *d*-orbital splitting between $GaCuO_2$ and $GaCu_{0.94}Fe_{0.06}O_2$.

3.5. Thermoelectric properties

The thermoelectric properties involve the change of heat with electronic transitions in the physical and chemical processes [63], change of energy in the biological and chemical process [64] and interaction among system, surrounding and environment [65]. Entropy, heat capacity, enthalpy and free energy are the important parts of thermodynamics, which allow physics and physical chemistry to participate in any system. Petersen et al. reported that entropy and enthalpy are closely related to each other while the entropy informs about the discharge condition of any substance. Figure 10(a,b) illustrates the total comparison of thermophysical properties of $GaCuO_2$ and $GaCu_{0.94}Fe_{0.06}O_2$ which are as well explained the both doped and undoped effect in Figure 10(c–f).

3.5.1. Entropy

Entropy is a significant concept in physics and chemistry and functional to other disciplines. In addition to cosmology and economics, in physics, it is a part of thermodynamics, as well as core part of physical chemistry. It is an extent of the disorder of a system. It also confers the exclusive property of a thermodynamic system, which founds the value changes depending on the amount of matter. In equations (1) and (2), entropy is typically denoted by the letter S and has units of joules per Kelvin ($J\,K^{-1}$) or $kg\,m^2\,S^{-2}\,K^{-1}$. A highly ordered system has low entropy. Figure 10(c) demonstrates that the Entropy of $GaCu_{0.94}Fe_{0.06}O_2$ is higher than $GaCuO_2$ at 500 K, and the most upper entropy peak is at 90 and 178 cm^{-1} for $GaCuO_2$ and $GaCu_{0.94}Fe_{0.06}O_2$, respectively. It has illustrated that the increase of temperature shows the increase of the entropy for both crystals. But, the value of entropy of $GaCu_{0.94}Fe_{0.06}O_2$ is higher than $GaCuO_2$ from low temperature to apex temperature. Consequently, it could be articulated that the material of $GaCuO_2$ shows less disordered behaviour or

Figure 8. (Colour online) Conductivity.
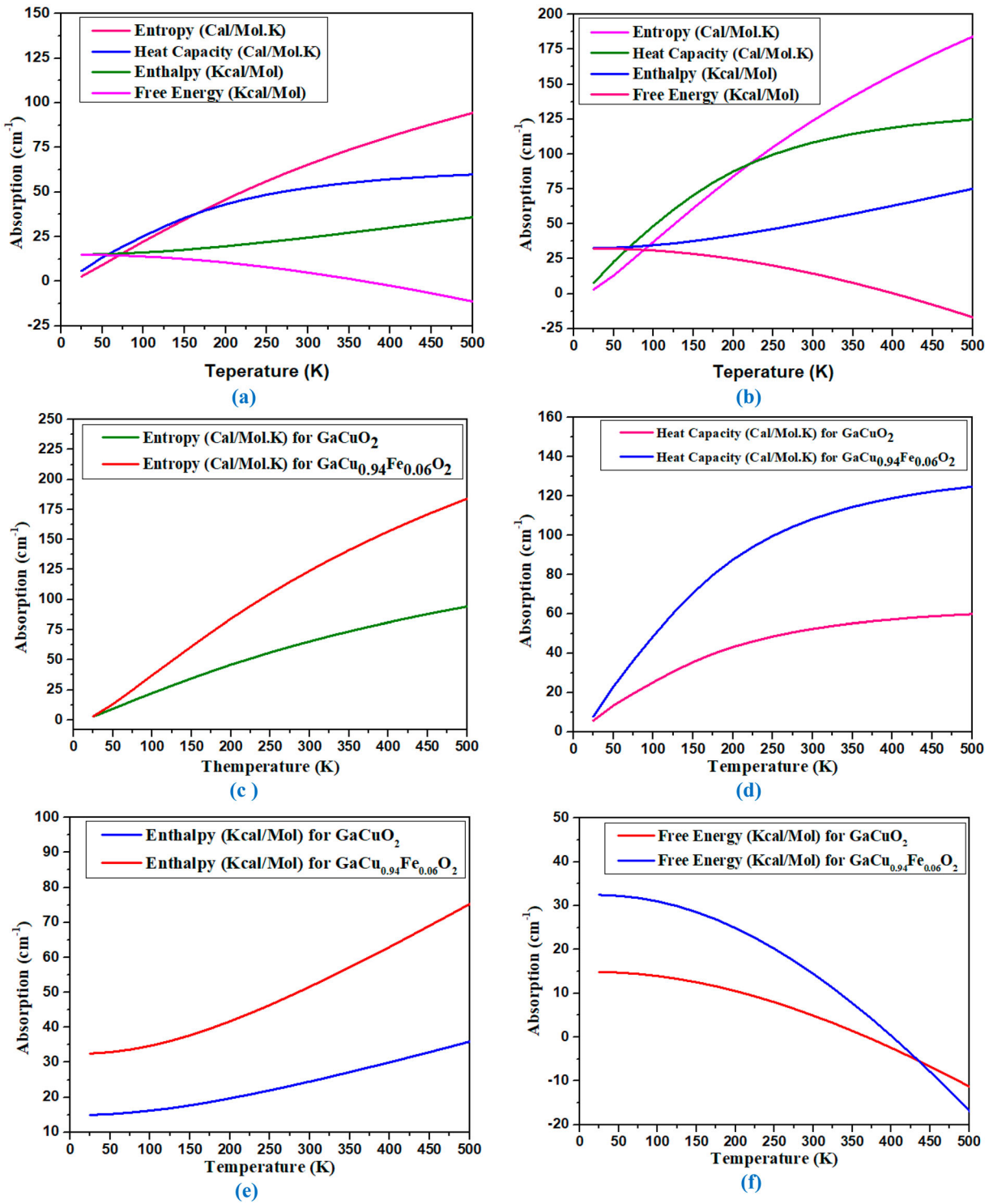
Figure 10. (Colour online) Thermodynamic properties of (a) GaCuO$_2$ and (b) GaCu$_{0.94}$Fe$_{0.06}$O$_2$; comparison of (c) total entropy, (d) total heat capacity, (e) total enthalpy and (f) total free energy.

molecular disturbances than GaCu$_{0.94}$Fe$_{0.06}$O$_2$. Besides, the conduction properties for GaCuO$_2$ and GaCu$_{0.94}$Fe$_{0.06}$O$_2$ are not as high as the other materials.

3.5.2. Heat capacity

Heat capacity is the magnitude of heat energy mandatory to raise the temperature of the body a particular amount. The

Table 2. Thermophysical properties of GaCuO$_2$ at different temperatures.

Compound name	Temperature (K)	Entropy (cal/mol K)	Heat capacity (cal/mol K)	Enthalpy (K cal/mol)	Free Energy (K cal/mol)
GaCuO$_2$	100	22.31	25.28	16.17	13.94
	273	60.52	50.30	23.37	6.65
	298	65.06	52.30	24.41	5.02
	323	68.88	54.02	25.23	3.86
	348	73.52	54.95	27.08	2.01
	373	77.24	55.88	28.01	0.15
	398	80.95	56.81	29.87	−1.70

Table 3. Thermophysical properties of GaCu$_{0.94}$Fe$_{0.06}$O$_2$ at different temperatures.

Compound name	Temperature (K)	Entropy (cal/mol K)	Heat capacity (cal/mol K)	Enthalpy (K cal/mol)	Free energy (K cal/mol)
GaCu$_{0.94}$Fe$_{0.06}$O$_2$	100	37.29	48.71	34.71	30.98
	273	113.86	103.83	48.66	18.57
	298	123.36	108.01	51.41	14.62
	323	132.26	112.19	53.68	11.88
	348	140.61	113.86	57.02	8.54
	373	148.97	115.54	60.37	5.20
	398	155.66	117.21	62.04	1.85

heat capacity of a material is affected by the existing force which makes high-ceilinged the complexity to the kinetic energy of a material. The heat properties of an alloy can vary dramatically from that of its component elements. As can be seen in Figure 10(d), the comparative study presents the total heat capacity of GaCuO$_2$ and GaCu$_{0.94}$Fe$_{0.06}$O$_2$. The heat capacity changes at a same rate, but in the case of GaCu$_{0.94}$Fe$_{0.06}$O$_2$, it is higher than GaCuO$_2$. After doping, 6% Fe doping (GaCu$_{0.94}$Fe$_{0.06}$O$_2$) demonstrates the increase of threefold than it origin which makes its rewarding material in optoelectronic devices.

3.5.3. Enthalpy

Enthalpy is a thermodynamic property which belongs to do the capacity to do non-mechanical work and the competence to discharge heat. The following equations are used to calculate the enthalpy.

$$H = E + PV \tag{1}$$

$$dH = TdS + PdV \tag{2}$$

Here, H is enthalpy, E is the internal energy of the system, P is pressure and V is volume.

From Figure 10(e), it is found that with increasing the temperature from 25 to 500K, the enthalpy change is obtained from 15 to 35 kcal/mol, respectively, for the GaCuO$_2$. Alternatively, the enthalpy change for GaCu$_{0.94}$Fe$_{0.06}$O$_2$ is higher than GaCuO$_2$ which is threefold than GaCuO$_2$ maintaining the uniform change with respect to temperature.

3.5.4. Free energy

Free energy refers to the amount of internal energy of a thermodynamic system that is available to perform work. In our investigation, it is observed that the free energy of GaCuO$_2$ and GaCu$_{0.94}$Fe$_{0.06}$O$_2$ inaugurates from around 15 and 32 cm^{-1}, respectively, at 25 K. Figure 10(f) explains that the free energy of GaCu$_{0.94}$Fe$_{0.06}$O$_2$ is higher than GaCuO$_2$ and the free energy has overlapped with the absorption level of -10 at the temperature of 425 K. After 425 K, this phenomenon has reversed.

Finally, the thermodynamic properties have been listed in Figure 10(a,b). Figure 10(c–f) indicates that the main parts of thermodynamic properties such as entropy, heat capacity, enthalpy and free energy for GaCuO$_2$ and GaCu$_{0.94}$Fe$_{0.06}$O$_2$. Eventually, from Figure 10(a–f), it is proved that the thermodynamic properties have changed after Fe doping. It could be concluded that the thermophysical properties of GaCuO$_2$ and GaCu$_{0.94}$Fe$_{0.06}$O$_2$ at different temperatures have been compared in Tables 2 and 3.

4. Conclusion

Although crystal or oxide of gallium was established as the wide band gap material for use in optoelectronic devices, it was found that GaCuO$_2$ was evaluated as narrow band gap material through the computational tools of the first principle method on the basis of DFT functionals. Firstly, the obtained band gap was at 0.756 eV by GGA with the PBE method. Secondly, the functionals of GGA with RPBE and LDA with CA-PZ were executed for comparative study and the values were 0.786 and 0.759 eV, respectively. Therefore, it could be revealed that the functionals of GGA with PBE, GGA with RPBE, and LDA with CA-PZ convey closer values of band gap and band structure containing Ga or Cu metals in crystals. Due to 6% Fe doping, the electronic band gap is decreased which is supported by the change of DOS and PDOS data whereas the total sum of DOS is increased by five times over the energy region. Thus, the d-orbital of Fe must articulate the best contributor for obtaining narrow band gap engineering. Moreover, the calculated band gap for GaCu$_{0.92}$Fe$_{0.08}$O$_2$ is turned into 0.00 eV using three DFT functionals. In the case of optical properties, the GaCu$_{0.92}$Fe$_{0.08}$O$_2$ is a superior material for the use of optoelectronic devices than GaCuO$_2$ regarding the pieces of evidence of absorption, reflectivity, loss function and conductivity. But slightly inverse results are found from entropy and free energy for GaCu$_{0.92}$Fe$_{0.08}$O$_2$ and GaCuO$_2$, because they illustrate a chemically and thermally less stable crystal in high temperature. After all, both GaCu$_{0.92}$Fe$_{0.08}$O$_2$ and GaCuO$_2$ demonstrate the perfect crystals at temperature 25 K.

ORCID

Debashis Howlader http://orcid.org/0000-0003-4149-971X
Md. Sayed Hossain http://orcid.org/0000-0003-4426-3956
Unesco Chakma http://orcid.org/0000-0003-1711-7216
Ajoy Kumer http://orcid.org/0000-0001-5136-6166
Mohammad Jahidul Islam http://orcid.org/0000-0002-4125-8222
Md. Tawhidul Islam http://orcid.org/0000-0002-5024-5781
Tomal Hossain http://orcid.org/0000-0002-8828-7282
Jahedul Islam http://orcid.org/0000-0002-5066-3828

References

[1] Davis E, Mott N. Conduction in non-crystalline systems V. Conductivity, optical absorption and photoconductivity in amorphous semiconductors. Philos Mag. 1970;22:0903–0922.

[2] Hudgins JLS, Grigory S, Santi E, et al. An assessment of wide band-gap semiconductors for power devices. IEEE Trans Power Electron. 2003;18:907–914.

[3] Huang XM, Chelikowsky JR, Kronik L. Size-dependent spintronic properties of dilute magnetic semiconductor nanocrystals. Phys Rev Lett.. 2005;94:236801.

[4] Awschalom DDF, Michael E. Challenges for semiconductor spintronics. Nat Phys. 2007;3:153–159.

[5] Fortunato EB, Pedro MR. Oxide semiconductor thin-film transistors: a review of recent advances. Adv Mater. 2012;24:2945–2986.

[6] Chilla JL, Butterworth A, Stuart D, et al. High-power optically pumped semiconductor lasers. In: Solid State lasers XIII: Technology and devices, San Jose, CA, 2004, pp. 143–150.

[7] Steven DTF, Smith L, Brazil B. Automated data collection using simple and inexpensive microcontrollers and semiconductor sensors. In: CHI '99 extended abstracts. New York (NY): ACM Press; 1999. doi:10.1145/632716.632938.

[8] Mario KJCB, Noh YY. Toward printed integrated circuits based on unipolar or ambipolar polymer semiconductors. Adv Mater. 2013;25:4210–4244.

[9] Jianquan JLD, Yang L, Zhang T, et al. Decoupling of thermo-electronic effect by traveling photothermal mirror method for characterization of thermal properties of semiconductors. Appl Phys Lett. 2020;116:114102.

[10] Hongwei AMDS, Rhyner MN, Ruan G, et al. A systematic examination of surface coatings on the optical and chemical properties of semiconductor quantum dots. Phys Chem Chem Phys. 2006;8:3895–3903.

[11] Sandra CEE, Avlicek M, Stadler P, et al. The role of heteroatoms leading to hydrogen bonds in view of extended chemical stability of organic semiconductors. Adv Funct Mater. 2015;25:6679–6688.

[12] Jie QXF, Zhang W, Song Y, et al. Physical properties of group 14 semiconductor alloys in orthorhombic phase. J Appl Phys. 2019;126:045709.

[13] Chakma U, Kumer A, Chakma KB, et al. Electronics structure and optical properties of $SrPbO_3$ and $SrPb_{0.94}Fe_{0.06}O_3$: a first principle approach. Eurasian Chem Commun. 2020;2:573–580.

[14] Chakma U, Kumer A, Chakma KB, et al. Electronics structure and optical properties of $Ag2BiO3,(Ag2)0.88Fe0.12BiO3$: a first principle approach. Adv J Chem Sect A Theor Eng Appl Chem. 2020;3:542–550.

[15] Hasan MM, Ajoy K, Chakma U. Theoretical investigation of doping effect of Fe for $SnWO_4$ in electronic structure and optical properties: DFT based first principle study. Adv J Chem Sect A. 2020;3:639–644.

[16] Islam MT, Ajoy K, Debashis HOWLADER, et al. Electronics structure and optical properties of $Mg(BiO_2)_4$ and $Mg(Bi_{0.91}Ge_{0.083}O_2)_4$: a first principle approach. Turkish Comput Theor Chem. 2020;4:24–31.

[17] Kamal BC, Ajoy K, Unesco C, et al. A theoretical investigation for electronics structure of $Mg(BiO_2)_2$ semiconductor using first principle approach. Int J New Chem. 2020;7:247–255.

[18] Kamal Bikash C, Ajoy K, Unesco C, et al. A theoretical investigation for electronics structure of $Mg(BiO_2)_2$ semiconductor using first principle approach. Int J New Chem. 2020;2020:247–255.

[19] Md Tawhidul Islam CD, Kumer A, Unesco H. A computational investigation of electronic structure and optical properties of $AlCuO_2$ and $AlCu_{0.96}Fe_{0.04}O_2$: a first principle approach. Orbital Electron J Chem. 2021;13:58–64.

[20] Leonardo SADS, Caroli E, Mancini AM, et al. Progress in the development of CdTe and CdZnTe semiconductor radiation detectors for astrophysical and medical applications. Sensors. 2009;9:3491–3526.

[21] Sebastién NRK, Dornfeld D. Quantifying the environmental footprint of semiconductor equipment using the environmental value systems analysis (EnV-S). IEEE Trans Semicond Manuf. 2004;17:554–561.

[22] Wu HK, Mansoor A, Hussain AS. Process control perspective for process analytical technology: integration of chemical engineering practice into semiconductor and pharmaceutical industries. Chem Eng Commun. 2007;194:760–779.

[23] Jingrun LRZ, Qiao S-Z, Jaroniec M. Characterization of semiconductor photocatalysts. Chem Soc Rev. 2019;48:5184–5206.

[24] Md Mahmud Hasan AU, Kumer C, Md TI. Structural, optical and electronic properties of $ZnAg_2GeTe_4$ and $ZnAg_2Ge_{0.93}Fe_{0.07}Te4$ photocatalyst: a first principle approach. Mol Simul. 2021;47:1–13.

[25] Islam MJ, Kumer A. First-principles study of structural, electronic and optical properties of $AgSbO_3$ and $AgSb_{0.78}Se_{0.22}O_3$ photocatalyst. SN Appl Sci. 2020;2:251.

[26] Chakma SUMM, Kumer A, Mohammad JI, et al. The exploration of structural, electronic and optical properties for $MoS2$ and $Mo0.95W0.05S2$ photocatalyst effort on wastewater treatment using DFT functional of first principle approach. App J Environ Eng Sci. 2021;7:103–113.

[27] Bholanath TPS, Huang J, Katz HE. Organic semiconductor devices with enhanced field and environmental responses for novel applications. MRS Bull. 2008;33:690–696.

[28] Dongge DMY. Development of organic semiconductor photodetectors: from mechanism to applications. Adv Opt Mater. 2019;7:1800522.

[29] Huanli CDW, Jiang L, Hu W. Organic semiconductor crystals. Chem Soc Rev. 2018;47:422–500.

[30] Samuel IDWT, Alexander G. Organic semiconductor lasers. Chem Rev.. 2007;107:1272–1295.

[31] Julian WSZ, Chigrinov VG, Kwok HS, et al. Optically addressable photoaligned semiconductor nanorods in thin liquid crystal films for display applications. Adv Opt Mater. 2018;6:1800250.

[32] Makoto MYO, Shimizu Y, Fujii A. Carrier transport and device applications of the organic semiconductor based on liquid crystalline non-peripheral octaalkyl phthalocyanine. Liq Cryst. 2018;45:2376–2389.

[33] Rüdiger AJMN. Physical chemistry of semiconductor−liquid interfaces. J Phys Chem. 1996;100:13061–13078.

[34] Addamiano A. Preparation and photoluminescence of Silicon carbide phosphors doped with group III a elements and/or nitrogen. J Electrochem Soc. 1966;113:134–136.

[35] Masahiro HYK, Hyodo H, Kurita M, et al. P-type electrical conduction in transparent thin films of $CuAlO_2$. Nature. 1997;389:939–942.

[36] RJ MINM. New structural systematics in the II–VI, III–V, and group-IV semiconductors at high pressure. Physica Status Solidi (b). 1996;198:389–402.

[37] Akira YTN, Tsubomura H. Efficient photoelectrochemical conversion of solar energy with N-type silicon semiconductor electrodes surface-doped with IIIA-Group elements. Chem Lett.. 1982;11:1071–1074.

[38] M. C. Saba C, Bloch J, Thierry-Mieg V, et al. High-temperature ultrafast polariton parametric amplification in semiconductor microcavities. Nature. 2001;414:731.

[39] Jung-Hun MSK, Singisetti U, Ma Z. Recent advances in free-standing single crystalline wide band-gap semiconductors and their applications: GaN, SiC, ZnO, β-Ga_2O_3, and diamond. J Mater Chem C. 2017;5:8338–8354.

[40] Aziz SB. Modifying poly (vinyl alcohol)(PVA) from insulator to small-bandgap polymer: A novel approach for organic solar cells and optoelectronic devices. J Electron Mater. 2016;45:736–745.

[41] Ali MI, Jahidul M, Rafid M, et al. The computational screening of structural, electronic, and optical properties for SiC, $Si_{0.94}Sn_{0.06}C$, and $Si_{0.88}Sn_{0.12}C$ lead-free photovoltaic inverters using DFT functional of first principle approach. Eurasian Chem Commun. 2021;3:327–338.

[42] Tomal Hossain AMSH, Ali MH, Chakma U, et al. Investigation of optoelectronics, thermoelectric, structural and photovoltaic properties of $CH_3NH_3SnBr_3$ lead-free organic perovskites. Chem Method. 2021;5:259–270.

[43] Ching-Hwa L-CHT. Synthesis, optical characterization, and environmental applications of β-Ga2O3 nanowires. Gallium Oxide Technol Dev Appl. 2019, pp. 67–90.

[44] Jiancheng SYP, Cary IV, Patrick H, et al. A review of Ga_2O_3 materials, processing, and devices. Appl Phys Rev. 2018;5:011301.

[45] Geller S. Crystal structure of β-Ga_2O_3. J Chem Phys. 1960;33:676–684.

[46] Akito MAKM, Calkins J, Kim J, et al. Perspective—opportunities and future directions for Ga_2O_3. ECS J Solid State Sci Technol. 2017;6:P356.

[47] Ju-Hee CSL, Muth J, Dickey MD. 3D printing of free standing liquid metal microstructures. Adv Mater. 2013;25:5081–5085.

[48] Rui MZH, Lam LS, Wilcoxon R, et al. On the potential of galinstan-based minichannel and minigap cooling. IEEE Trans Compon, Packag Manuf Technol. 2013;4:46–56.

[49] Khondoker M, Sameoto D. Fabrication methods and applications of microstructured gallium based liquid metal alloys. Smart Mater Struct. 2016;25:093001.

[50] Hiroshi JCAW, Hanks CT, Okabe T. Correlation of cytotoxicity with elemental release from mercury-and gallium-based dental alloys in vitro. Dent Mater. 1994;10:298–303.

[51] V. M. Volkovich DS, Yamshchikov LF, Chukin AV, et al. Thermodynamic properties of uranium in gallium–aluminium based alloys. J Nucl Mater. 2015;465:153–160.

[52] A. S. Shubin KY, Yamshchikov LF. The diffusion of gallium into copper-tin alloy particles. *Defect Diffus Forum*. 2009;283–286:238–242.

[53] Ramanujam JS, Udai P. Copper indium gallium selenide based solar cells – a review. Energy Environ Sci. 2017;10:1306–1319.

[54] Ajoy K, Chakma U. Developing the amazing photocatalyst of $ZnAg_2GeSe_4$, $ZnAg_2Ge_{0.93}Fe_{0.07}Se_4$ and $ZnAg_2Ge_{0.8}6Fe_{0.14}Se_4$

[55] Kieron JPBP, Ernzerhof M. Generalized gradient approximation made simple. Phys. Rev. Lett. 1996;77:3865.

[56] del Campo JMG, José L, Trickey SB, et al. Non-empirical improvement of PBE and its hybrid PBE0 for general description of molecular properties. J Chem Phys. 2012;136:104108.

[57] I. B. Aanouz A, El-Khatabi K, Lakhlifi T, et al. Moroccan medicinal plants as inhibitors against SARS-CoV-2 main protease: computational investigations. J Biomol Struct Dyn. 2020;39:2971–2979. doi:10.1080/07391102.2020.1758790,.

[58] Roberto AMOF, Rérat M. Ab initio calculation of the ultraviolet–visible (UV-vis) absorption spectrum, electron-loss function, and reflectivity of solids. J Chem Theory Comput. 2015;11:3245–3258.

[59] Debasish PBK, Cohen RE, Rubner MF. Structural color via layer-by-layer deposition: layered nanoparticle arrays with near-UV and visible reflectivity bands. J Mater Chem. 2009;19:8920–8927.

[60] A. M. A. Al Mamun M, Habib A, Chakma U, et al. Structural, electronic, optical properties and molecular dynamics study of WO_3 $W_{0.97}Ag_{0.03}O_3$ and $W_{0.94}Ag_{0.06}O_3$ photocatalyst by the first principle of DFT study. Egypt J Chem. 2021;63:5117–5126.

[61] T. N. M. Duy J, Pichard G. CMT: the material for fiber optical communication devices. J Cryst Growth. 1985;72:490–495.

[62] Jes JCBK, Birks TA, Russell PSJ. Photonic band gap guidance in optical fibers. Science. 1998;282:1476–1478.

[63] Smith JM. Introduction to chemical engineering thermodynamics. New York: ACS Publications; 1950.

[64] Kaufman L, Cohen M. Thermodynamics and kinetics of martensitic transformations. Prog Metal Phys. 1958;7:165–246.

[65] Shapiro AH. The dynamics and thermodynamics of compressible fluid flow. New York: Wiley; 1953.